Hindawi
Journal of Nanomaterials
Volume 2022, Article ID 1915185, 15 pages
https://doi.org/10.1155/2022/1915185

Research Article

Entropy Analysis in Bidirectional Hybrid Nanofluid Containing Nanospheres with Variable Thermal Activity

Iftikhar Ahmad,[1] Qazi Zan-Ul-Abadin,[1] Muhammad Faisal,[1] K. Loganathan,[2,3] Tariq Javed,[4] and Sonam Gyeltshen[5]

[1]*Department of Mathematics, Azad Jammu & Kashmir University, Muzaffarabad 13100, Pakistan*
[2]*Research and Development Wing, Live4Research, Tiruppur, 638106 Tamil Nadu, India*
[3]*Department of Mathematics and Statistics, Manipal University Jaipur, Jaipur, 303007 Rajasthan, India*
[4]*Department of Mathematics and Statistics, International Islamic University, Islamabad 44000, Pakistan*
[5]*Department of Humanities and Management, Jigme Namgyel Engineering College, Royal University of Bhutan, Dewathang, Bhutan*

Correspondence should be addressed to Muhammad Faisal; muhamamd.faisal@ajku.edu.pk, K. Loganathan; loganathankaruppusamy304@gmail.com, and Sonam Gyeltshen; sonamgyeltshen@jnec.edu.bt

Received 19 May 2022; Revised 18 June 2022; Accepted 5 July 2022; Published 18 July 2022

Academic Editor: Hafiz Muhammad Ali

An investigation of the thermal performance of water-conveying nanospheres (magnetite (Fe_3O_4) and silver (Ag)) subject to variable thermal controls, namely, variable surface temperature and variable surface normal heat flux, has been made. A bidirectionally elongating surface is used to generate an unsteady flow mechanism with the action of the Lorentz force. Derived equations of basic laws are firstly nondimensionalized and then numerically solved by applying the Keller-Box method. The local Nusselt number for both the thermal cases is calculated and discussed. Percent-wise enhancement in the rate of heat transport has also been included in the analysis. It was concluded through the present exploration that at lower volume fractions of magnetite and silver, the rate of heat transport is observed to be dominant. The rate of heat transference has attained identical values for both the provided thermal conditions at the surface. Moreover, intensities of velocity and thermal profiles diminish with the appreciation of the choice of unsteadiness. The temperature-controlling indices also affect the thermal profile, and it is reduced with the intensification in the considerations of these indices. The values of thermal conductivity, density, and electrical conductivity have been improved with the inclusion of nanospheres (magnetite (Fe_3O_4) and silver (Ag)), whereas the value of specific heat is reduced with the mixture of these nanospheres. The Nusselt number is increased up to 5% with the involvement of magnetite nanospheres, and it is enhanced up to 4% with the involvement of silver nanospheres.

1. Introduction

A staggering and unprecedented advancement in the field of microelectronics, microfluidics, chemical synthesis, optical devices, high-power engines, shipping, microsystems, and electrical and mechanical components has entirely transformed the foundations of human life. These developments additionally demand effective cooling procedures in order to explore the performance of thermal conductivity and reliability of operational devices. The basic idea of controlling the thermal efficiency via cooling through fluids seems to be deficient, and hence, this issue has been resolved by submerging the tiny particles into the host fluid that certainly affects its thermomechanical possessions. This colloidal mixture of tiny particles into the host fluid is famous for the name nanofluid. Famous theoretical models regarding the study of thermal conductivity have been proposed by Choi et al. [1], Maxwell [2], and Bruggeman [3]. The pioneer nanofluid model for the study of tiny particle shapes/sizes is presented by Hamilton and Crosser [4], and it shows that the shapes of the dispersed tiny particles sufficiently affect the thermophysical behavior of heterogeneous substances.

Later on, Masoumi et al. [5] presented the model to compute the operative viscosity of nanomaterials. The development of knowledge in the field of nanofluid has also led us to the understanding of tiny particle shapes/sizes as an important factor causing changes in thermal conductivity and viscosity. Some more recent developments in the existing nanofluid models regarding the shapes/sizes of nanoparticles are disclosed by Mooney [6] and Ohshima [7]. In these nanofluid models, it is inferred that the thermal conductivity performance of water-conveying nanomaterial is significantly improved by submerging the nanospheres. Some more extraordinary explorations regarding the control of the nanoparticle shape factor on the thermal executions of various substances are made by the researchers via Refs. [8–12].

Recently, an improved class of nanofluids with the name hybrid nanofluid has come into existence to bear the high performance of thermal conductivity associated with the mono-nanofluid. With the utilization of hybrid nanofluids, revolutionary applications in the field of heat transfer processes are found in generator and nuclear cooling systems, automobile radiators, electronic cooling with coolants in the machinery, solar heating, welding, lubrication, drug reduction, biomedicine, cooling and heating in buildings, and defense. The main issue for the regular nanofluid network is that they either have a good thermal conductive performance or have a better rheological setup. Single-handedly, they do not possess all the necessary properties which are mandatory for a certain heat exchanger application. Therefore, with the suitable choice of two or more nanoparticles, hybrid nanofluid can provide us with a well-suited mixture, which owns all physicochemical features of different substances that can scarcely be found in a separate substance. These distinctive properties of hybrid nanofluids have increased the attention of worldwide investigators, and therefore, many research articles have been published in this fascinating field over the last decade. Numerical exploration regarding the 3D flow of hybrid nanofluid $(Cu - Al_2O_3/H_2O)$ towards an expanding obstacle with the significance of the Newtonian heating and Lorentz force is made by Devi and Devi [13] and obtained that the frequency of heat transference for the hybrid nanofluid is much better than that for the ordinary nanofluid even with the effect of the magnetic environment. Hayat et al. [14] conferred the 3D radiative dynamics of hybrid nanofluid $(Ag - CuO/H_2O)$ impinging over a bidirectionally expanding slippery surface in a rotating frame and concluded that the rate of heat transference of the hybrid nanofluid is improved as compared to that of the traditional nanofluid. The detailed analysis of the thermal conductivity and viscosity of hybrid nanofluid $(Al_2O_3 - CuO)$ with ethylene glycol and propylene glycol binary host fluid with different shapes of nanoparticles (i.e., spherical, cylindrical, platelet, blade, and brick) is disclosed by Kumar and Sahoo [15] and concluded that the nanoparticles having spherical shapes have two percent higher thermal conductivity to that of platelet-shaped nanoparticles. Moreover, the impact of volume fraction on nanoparticles is detected incredibly in the thermal conductivity of nanofluids. Nabil et al. [16] comprehensively discussed the thermophysical features of hybrid nanofluids and hybrid nanolubricants with potential applications in the engineering sector with the predictions of their future utilization. Rashid and Liang [17] presented the numerical solution for the dynamics of MHD nanofluid with the significance of different shapes of nanoparticles over a rotating stretchable obstacle through a porous domain. A theoretical investigation regarding the transitory steady flow of water-conveying hybrid nanofluid containing magnetite and silver nanospheres is conducted by Nabwey and Mahdy [18]. Zainal et al. [19] numerically explored the impact of MHD on the steady bidirectional flow of hybrid nanofluid containing copper and aluminum oxide nanoparticles with water as host fluid. Besides, many researchers [20–25] have contributed to the field of hybrid nanofluid with various thermal engineering aspects.

Passive/variable thermal aspects play a significant role in the development of aircraft cooling frames, heat exchanger devices, fuselage condensation processes, air conditioning condensers, refrigeration systems, electric heaters, power converters, motor controllers, and many other industrial and mechanical applications. Oliveira et al. [26] presented a design for a passive heat exchanger system to control the cooling system of aircraft for variable thermal conditions. In this investigation, water is considered a host liquid with the features of natural, forced, and mixed convection. The aspects of passive heating on the dynamics of fluid in the boundary layer zone are initially discussed by Liu and Andersson [27] by considering the variable surface temperature (VST) and variable surface heat flux (VHF) mechanisms. The rate of heat transference is expressively enhanced with the presence of these heating mechanisms. Ahmad et al. [28] numerically disclosed the unsteady 3D flow of copper-water nanofluid with variable thermal aspects. Ahmad et al. [29] also reported the unsteady 3D rotating flow of nanofluid with the aspects of the prescribed thermal environment. The hybrid nanofluid flow over an expanding cylinder with the characteristic of prescribed surface heat flux is examined by Waini et al. [30]. Waini et al. [31] also disclosed the significance of prescribed surface heat flux on the dynamics of hybrid nanofluid past over a thin needle. Khashi'ie et al. [32] discussed the flow of hybrid nanofluid over a shrinking domain with prescribed thermal conditions. The effect of suspended particles on the flow of nanofluid with the effect of VST and VHF mechanisms is also analyzed by Gireesha et al. [33]. Some leading explorations regarding the outcomes of prescribed thermal conditions on the flow of nanofluids as well as hybrid nanofluids are found via Refs. [34–37].

Entropy is a physical property of the system that obeys the thermodynamic second law. It measures the level of disorderliness and unproductive energy within the environment. The entropy of a reversible system is constant, whereas the entropy of an irreversible system varies with the factors involved in transport equations. In general, real processes are reversible (i.e., the system responds according

to the environmental scenario). Entropy transport in hybrid nanofluid is a new area of research and got considerable importance nowadays. Entropy transport in nanofluids as well as hybrid nanofluids within the thermal environment is inquired by Huminic and Huminic [38]. Khan et al. [39] scrutinized the entropy transport in the rotatory flow of hybrid nanofluid influenced by magnetization. Heat transport and entropy transport in hybrid nanofluids packed in a flattened tube are examined by Huminic and Huminic [40]. Entropy transport with temperature-controlled viscosity in hybrid nanofluid comprising single-walled as well as multiwalled carbon nanotubes is elaborated by Ahmad et al. [41]. Entropy transport in the peristaltic-type flow of hybrid nanofluid is reported by Zahid et al. [42]. Hussien et al. [43] discussed the entropy and thermal transport in hybrid nanofluids by considering microtubes. Sheikholeslami et al. [44] considered the entropy transport in hybrid nanofluid contained in a porous tank with the impact of the Lorentz force. Heat and entropy transport assessment in the bidirectional flow of hybrid nanofluid by the movement of convectively heating devices is disclosed by Upreti et al. [45]. Saleh and Sundar [46] focused on entropy and exergy transport in hybrid nanofluid containing nanodiamond in a circular tube. Recently, Eswaramoorthi et al. [47] investigated the entropy and heat transport in magnetized water-driven nanofluid over a bidirectional moving device with a radiation phenomenon.

The above literature survey reveals the statement that no attention has been given in order to investigate the unsteady 3D entropy optimized flow of water-based hybrid nanofluid containing nanospheres, i.e., magnetite and silver, towards an elongating surface with passive thermal controls. The effect of the Lorentz force is also considered in the modeling for physical relevancy. A passive heat controlling system consists of both variable surface temperature and variable surface heat flux mechanisms. Similarity transformations have been used to accomplish the mathematical model for solvable situations. The Keller-Box method [48–52] with Newton's linearization scheme has been endorsed to find the numerical solution of the modeled problem. The validity of the acquired results is discussed through the grid-independent tactic. The graphical aids have been provided to discuss the influence of various emerging entities on thermal as well as entropy setups. The relations based on the coefficient of skin friction, entropy formation, Bejan number, and local Nusslet number have also been derived and discussed through various scientific patterns.

2. Mathematical Formulation

The mathematical formulation of the problem has been completed in view of the undermentioned assumptions:

(i) Incompressible, laminar, and unsteady flow

(ii) Bidirectional stretching

(iii) Thermal equilibrium situation of nanospheres (i.e., magnetite and silver) with water

(iv) No-slip condition at the surface within the boundary layer region

(v) Utilization of variable thermal conditions

(vi) Magnetohydrodynamic three-dimensional flow

(vii) Entropy and heat transport

2.1. Flow Description. The Cartesian configuration is used to frame an unsteady mathematical model regarding the dynamics of hybrid nanofluid containing nanospheres (Fe_3O_4 and Ag) suspended in water towards a bidirectionally elongating surface. Magnetite nanospheres can be used in the process of water purification, drug delivery, and steel manufacturing, whereas silver is the best electrical as well as thermal conductor among all metals and hence ideal for electrical applications. The concept of variable magnetic field $B(t) = B_0/\sqrt{1-ct}$ having strength B_0 is externally applied through the Lorentz force in the absence of an electric field. The nanospheres are in thermal equilibrium with the base liquid. The concept of the no-slip condition at the surface within the boundary stream is also utilized for laminar and incompressible flow. The hybrid nanofluid is restricted in the domain $0 < z < \infty$, whereas the disturbance in the hybrid nanofluid is created through expansion velocity $u_w = ax/(1-ct)(a > 0, c > 0)$ along the x-direction and expansion velocity $v_w = by/(1-ct)(b \geq 0)$ along the y-direction of the system configuration (as shown in Figure 1). The thermophysical properties of water H_2O, magnetite Fe_3O_4, and silver Ag are included in the mathematical modeling through Table 1.

In view of the aforementioned assumptions, component forms of governing equations are composed as (Ref. [12])

$$\frac{\partial u}{\partial x} + \frac{\partial v}{\partial y} + \frac{\partial w}{\partial z} = 0, \tag{1}$$

$$\frac{\partial u}{\partial t} + u\frac{\partial u}{\partial x} + v\frac{\partial u}{\partial y} + w\frac{\partial u}{\partial z} = \frac{\mu_{hnf}}{\rho_{hnf}}\frac{\partial^2 u}{\partial z^2} - \frac{\sigma_{hnf}}{\rho_{hnf}}B(t)^2 u, \tag{2}$$

$$\frac{\partial v}{\partial t} + u\frac{\partial v}{\partial x} + v\frac{\partial v}{\partial y} + w\frac{\partial v}{\partial z} = \frac{\mu_{hnf}}{\rho_{hnf}}\frac{\partial^2 v}{\partial z^2} - \frac{\sigma_{hnf}}{\rho_{hnf}}B(t)^2 v, \tag{3}$$

with (Ref. [9])

$$\begin{aligned}
\rho_{hnf} &= \psi_1\rho_{p1} + \psi_2\rho_{p2} + (1-\psi_1-\psi_2)\rho_f,\\
\frac{\sigma_{hnf}}{\sigma_{bf}} &= 1 + \frac{3\left(\left(\sigma_{p2}/\sigma_{bf}\right)-1\right)\psi_2}{\left(\sigma_{p2}/\sigma_{bf}\right)+2-\left(\left(\sigma_{p2}/\sigma_{bf}\right)-1\right)\psi_2},\\
\frac{\sigma_{bf}}{\sigma_f} &= 1 + \frac{3\left(\left(\sigma_{p1}/\sigma_f\right)-1\right)\psi_1}{\left(\sigma_{p1}/\sigma_f\right)+2-\left(\left(\sigma_{p1}/\sigma_f\right)-1\right)\psi_1},\\
\frac{\mu_{hnf}}{\mu_{bf}} &= 1 + 2.5\psi_2 + 6.2{\psi_2}^2,\\
\frac{\mu_{bf}}{\mu_f} &= 1 + 2.5\psi_1 + 6.2{\psi_1}^2.
\end{aligned} \tag{4}$$

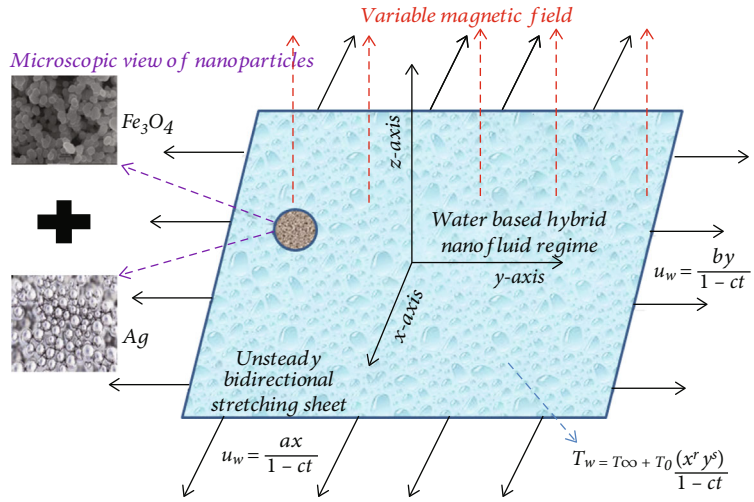

Figure 1: Graphical abstract of the mathematical model.

Table 1: Thermophysical features of water, magnetite nanoparticles, and silver nanoparticles (Ref. [20]).

Thermophysical features	Base fluid	Nanoparticles	
	H_2O	$Fe_3O_4(\psi_1)$	$Ag(\psi_2)$
Density: ρ (kgm^{-3})	997.1	5180	10500
Thermal conductivity: k ($Wm^{-1}K^{-1}$)	0.613	9.7	429
Specific heat: C_p ($Jkg^{-1}K^{-1}$)	4179	670	235
Electrical conductivity: σ ($\Omega^{-1}m^{-1}$)	0.05	2.5×10^4	6.3×10^7
Prandtl number: Pr	6.20	—	—

Supported BCs are (Ref. [34])

$$z = 0 : u = u_w(x,t) = \frac{ax}{1-ct}, v = v_w(y,t) = \frac{by}{1-ct}, w = 0, \tag{5}$$

$$z \longrightarrow \infty : u \longrightarrow 0, v \longrightarrow 0. \tag{6}$$

Similarity variables comprise (Ref. [35])

$$u = \frac{ax}{1-ct} f'(\eta), \tag{7}$$

$$v = \frac{ay}{1-ct} g'(\eta), \tag{8}$$

$$w = -\left(\frac{a\vartheta_f}{1-ct}\right)^{1/2} [f(\eta) + g(\eta)], \tag{9}$$

$$\eta = \left(\frac{a}{\vartheta_f(1-ct)}\right)^{1/2} z. \tag{10}$$

In the application of equation (7), equation (1) is identically balanced and equations (2)–(5) are of the following forms:

$$\varepsilon_1 f''' - f'^2 + (f+g)f'' - S\left(f' + \frac{\eta}{2}f''\right) - \varepsilon_2 M^2 f' = 0,$$
$$\varepsilon_1 g''' - g'^2 + (f+g)g'' - S\left(g' + \frac{\eta}{2}g''\right) - \varepsilon_2 M^2 g' = 0, \tag{11}$$

with

$$f(0) + g(0) = 0, \tag{12}$$

$$f'(0) = 1, \tag{13}$$

$$g'(0) = \alpha, \tag{14}$$

$$f'(\infty) \longrightarrow 0, \tag{15}$$

$$g'(\infty) \longrightarrow 0. \tag{16}$$

In the bidirectional flow, authors are generally concentrating on choosing the range of α as $0 < \alpha < 1$ because for $\alpha > 1$, the axes x and y are interchanged, and for $\alpha = 1$, the stretching rate becomes alike in both directions; thus, the flow profile turns out to be axisymmetric. Also, considering the limiting situation (i.e., $\alpha \longrightarrow 0$), the flow becomes unidirectional. Wang [53] reported that without any loss of generality, the condition $f(0) + g(0) = 0$ can be restored by $f(0) = 0$ and $g(0) = 0$. Further, in equations (1)–(12), velocity measures corresponding to the (x, y, z)-directions are (u, v, w), respectively. The presence

of time is denoted by t, whereas the temperature is symbolized by T, and hnf stands for the hybrid nanofluid, bf symbolizes the base fluid, nf discusses the nanofluid, μ expresses the viscosity, ρ reports the density, σ evokes the electrical conductivity, p_1 depicts the magnetite nanoparticles having concentration ψ_1, p_2 illustrates the silver nanoparticles having concentration ψ_2, and (f, g, η) posts the similarity variables with the involvement of ϑ_f (i.e., kinematic viscosity). Moreover, $S = c/a$, $M = (\sigma_f/a\rho_f)^{1/2}B_0$, and $\alpha = b/a$ diagnose the unsteady, magnetic, and expansion ratio parameters, respectively. The coefficients ε_1 and ε_2 are communicated as (Refs. [9, 12])

$$\varepsilon_1 = \frac{\left(1 + 2.5\psi_2 + 6.2{\psi_2}^2\right)\left(1 + 2.5\psi_1 + 6.2{\psi_1}^2\right)}{\left(\psi_1\left(\rho_{p1}/\rho_f\right) + \psi_2\left(\rho_{p2}/\rho_f\right) + (1 - \psi_1 - \psi_2)\right)},$$

$$\varepsilon_2 = \frac{\left(1 + \left(3\left(\left(\sigma_{p2}/\sigma_{bf}\right) - 1\right)\psi_2/\left(\left(\sigma_{p2}/\sigma_{bf}\right) + 2 - \left(\left(\sigma_{p2}/\sigma_{bf}\right) - 1\right)\psi_2\right)\right)\right)\left(1 + \left(3\left(\left(\sigma_{p1}/\sigma_f\right) - 1\right)\psi_1/\left(\left(\sigma_{p1}/\sigma_f\right) + 2 - \left(\left(\sigma_{p1}/\sigma_f\right) - 1\right)\psi_1\right)\right)\right)}{\psi_1\left(\rho_{p1}/\rho_f\right) + \psi_2\left(\rho_{p2}/\rho_f\right) + (1 - \psi_1 - \psi_2)}. \tag{17}$$

2.2. Heat Transport. In the current model, the heat transport phenomenon can be described by the following equation:

$$\frac{\partial T}{\partial t} + u\frac{\partial T}{\partial x} + v\frac{\partial T}{\partial y} + w\frac{\partial T}{\partial z} = \frac{k_{hnf}}{\left(\rho C_p\right)_{hnf}}\frac{\partial^2 T}{\partial z^2}, \tag{18}$$

with (Ref. [9])

$$\begin{aligned}\left(\rho C_p\right)_{hnf} &= \psi_1\left(\rho C_p\right)_{p1} + \psi_2\left(\rho C_p\right)_{p2} + (1 - \psi_1 - \psi_2)\left(\rho C_p\right)_f,\\ \frac{k_{hnf}}{k_{bf}} &= \frac{\left(k_{p2} + 2k_{bf}\right) + 2\psi_2\left(k_{p2} - k_{bf}\right)}{\left(k_{p2} + 2k_{bf}\right) - \psi_2\left(k_{p2} - k_{bf}\right)},\\ \frac{k_{bf}}{k_f} &= \frac{\left(k_{p1} + 2k_f\right) + 2\psi_1\left(k_{p1} - k_f\right)}{\left(k_{p1} + 2k_f\right) - \psi_1\left(k_{p1} - k_f\right)}.\end{aligned} \tag{19}$$

Here, two types of thermal BCs are used to discuss the variable thermal activity. These are variable surface temperature (VST) and variable surface heat flux (VHF). Mathematically, we have

$$\begin{aligned}&\text{VST case} : z = 0 : T = T_w(x, y, t) = T_\infty + T_0\left(\frac{x^r y^s}{1 - ct}\right), z \longrightarrow \infty : T \longrightarrow T_\infty,\\ &\text{VHF case} : z = 0 : -k_f\left(\frac{\partial T}{\partial z}\right)_w = q_w(x, y, t) = T_1\left(\frac{x^r y^s}{1 - ct}\right), z \longrightarrow \infty : T \longrightarrow T_\infty.\end{aligned} \tag{20}$$

Similarity transformations for both the thermal activities are (Ref. [12])

$$\text{VST case} : \theta(\eta) = \frac{T(x, y, z, t) - T_\infty}{T_w(x, y, t) - T_\infty}, \tag{21}$$

$$\text{VHF case} : T - T_\infty = \frac{T_1}{k_f}\left(\frac{\vartheta_f}{a(1 - ct)}\right)^{1/2} x^r y^s \phi(\eta). \tag{22}$$

As an application of equation (21), we have

$$\begin{aligned}&\text{VST case} : \varepsilon_3\theta'' + \Pr\left((f + g)\theta' - \left(rf' + sg'\right)\theta - S\left(\theta + \frac{\eta}{2}\theta'\right)\right) = 0,\\ &\text{VHF case} : \varepsilon_3\phi'' + \Pr\left((f + g)\phi' - \left(rf' + sg'\right)\phi - S\left(\phi + \frac{\eta}{2}\phi'\right)\right) = 0,\end{aligned} \tag{23}$$

with

$$\theta(0) = 1, \tag{24}$$

$$\phi'(0) = -1, \tag{25}$$

$$\theta(\infty) \longrightarrow 0, \tag{26}$$

$$\phi(\infty) \longrightarrow 0. \tag{27}$$

In equations (18)–(24), the free stream temperature is specified by T_∞, whereas (T_0, T_1) are dimensional constants. The variation in the surface temperature is controlled by the indices (r, s) along the (x, y)-directions, respectively. Thermal conductivity and specific heat capacitance are conveyed by k and ρC_p, respectively. The Prandtl number is expressed by $\Pr = \left(\rho C_p\right)_f \upsilon_f/k_f$, and the coefficient ε_3 may be expressed as

$$\varepsilon_3 = \frac{\left(\left(\left(k_{p2} + 2k_{bf}\right) + 2\psi_2\left(k_{p2} - k_{bf}\right)\right)/\left(\left(k_{p2} + 2k_{bf}\right) - \psi_2\left(k_{p2} - k_{bf}\right)\right)\right)\left(\left(\left(k_{p1} + 2k_f\right) + 2\psi_1\left(k_{p1} - k_f\right)\right)/\left(\left(k_{p1} + 2k_f\right) - \psi_1\left(k_{p1} - k_f\right)\right)\right)}{\psi_1\left(\left(\rho C_p\right)_{p1}/\left(\rho C_p\right)_f\right) + \psi_2\left(\left(\rho C_p\right)_{p2}/\left(\rho C_p\right)_f\right) + (1 - \psi_1 - \psi_2)}. \tag{28}$$

2.3. Entropy Transport. The equation that represents the entropy transport (ET) in the present situation may be expressed as

$$\begin{aligned} \mathrm{ET} = {} & \frac{k_{\mathrm{hnf}}}{T_\infty{}^2}\left[\left(\frac{\partial T}{\partial x}\right)^2 + \left(\frac{\partial T}{\partial y}\right)^2 + \left(\frac{\partial T}{\partial z}\right)^2\right] \\ & + \frac{\sigma_{\mathrm{hnf}} B(t)^2}{T_\infty}\left[u^2 + v^2\right] \\ & + \frac{\mu_{\mathrm{hnf}}}{T_\infty}\left[\left(\frac{\partial u}{\partial z}\right)^2 + \left(\frac{\partial v}{\partial z}\right)^2\right]. \end{aligned} \tag{29}$$

In equation (29), the first term is due to the heat transport and the second term is due to the magnetic field. It is appropriate to formulate the entropy transport as a factor form of the entropy transport (ET) rate and characteristic entropy (E_c) rate. Characteristic entropy for both the thermal regulations is defined as

$$\begin{aligned} E_{c1} &= \left.\frac{k_{\mathrm{hnf}}(T_w - T_\infty)^2}{T_\infty{}^2 x^2}\right|_{\mathrm{VST\ case}}, \\ E_{c2} &= \left.\frac{k_{\mathrm{hnf}}(T - T_\infty)^2}{T_\infty{}^2 x^2}\right|_{\mathrm{VHF\ case}}. \end{aligned} \tag{30}$$

2.3.1. Local Entropy Transport for the VST Case. The local entropy transport in dimensionless form for the VST case can be calculated as

$$\begin{aligned} \mathrm{ET}_1 = \frac{\mathrm{ET}}{E_{c1}} = {} & \mathrm{Re}_x \theta'^2 + r^2\theta^2 + s^2\theta^2 + \frac{\mathrm{Re}_x B_r}{\alpha_1} \\ & \cdot \left[M\varepsilon_4 f'^2 + \varepsilon_5 f''^2\right] + \frac{\mathrm{Re}_y B_r}{\alpha_1}\left[M\varepsilon_4 g'^2 + \varepsilon_5 g''^2\right]. \end{aligned} \tag{31}$$

Here, $B_r = \mu_f u_w{}^2/k_f(T_w - T_\infty)$ constitutes the Brinkman number, $\alpha_1 = (T_w - T_\infty)/T_\infty$ organizes the temperature difference parameter, and $(\varepsilon_4, \varepsilon_5)$ are due to the hybrid mixture of nanoparticles, and these may be expressed as

$$\varepsilon_4 = \frac{\left(1 + \left(3\left(\left(\sigma_{p2}/\sigma_{\mathrm{bf}}\right) - 1\right)\psi_2/\left(\left(\sigma_{p2}/\sigma_{\mathrm{bf}}\right) + 2 - \left(\left(\sigma_{p2}/\sigma_{\mathrm{bf}}\right) - 1\right)\psi_2\right)\right)\right)\left(1 + \left(3\left(\left(\sigma_{p1}/\sigma_f\right) - 1\right)\psi_1/\left(\left(\sigma_{p1}/\sigma_f\right) + 2 - \left(\left(\sigma_{p1}/\sigma_f\right) - 1\right)\psi_1\right)\right)\right)}{\left(\left(\left(k_{p2} + 2k_{\mathrm{bf}}\right) + 2\psi_2\left(k_{p2} - k_{\mathrm{bf}}\right)\right)/\left(\left(k_{p2} + 2k_{\mathrm{bf}}\right) - \psi_2\left(k_{p2} - k_{\mathrm{bf}}\right)\right)\right)\left(\left(\left(k_{p1} + 2k_f\right) + 2\psi_1\left(k_{p1} - k_f\right)\right)/\left(\left(k_{p1} + 2k_f\right) - \psi_1\left(k_{p1} - k_f\right)\right)\right)}, \tag{32}$$

$$\varepsilon_5 = \left(1 + 2.5\psi_1 + 6.2\psi_1{}^2\right)\left(1 + 2.5\psi_2 + 6.2\psi_2{}^2\right). \tag{33}$$

2.3.2. Local Entropy Transport for the VHF Case. The local entropy transport in dimensionless form for the VHF case can be calculated as

$$\begin{aligned} \mathrm{ET}_2 = \frac{\mathrm{ET}}{E_{c2}} = {} & \mathrm{Re}_x \phi'^2 + r^2\phi^2 + s^2\phi^2 + \frac{\mathrm{Re}_x B_r}{\alpha_1}\left[M\varepsilon_4 f'^2 + \varepsilon_5 f''^2\right] \\ & + \frac{\mathrm{Re}_y B_r}{\alpha_1}\left[M\varepsilon_4 g'^2 + \varepsilon_5 g''^2\right]. \end{aligned} \tag{34}$$

2.4. Physical Quantities. The key expressions for thermal engineering importance and heat exchanger devices are the skin friction coefficients (i.e., C_{fx} and C_{fy}) for the measurement of applied stresses at the wall, local Nusslet number (i.e., Nu_x) for the measurement of the rate of heat transference through the surface, and Bejan number (Be) for the measurement of irreversibility distribution. These engineering expressions are calculated through the following relations:

$$C_{fx} = \frac{\tau_{wx}}{\rho_f u_w{}^2},$$

$$C_{fy} = \frac{\tau_{wy}}{\rho_f v_w{}^2},$$

$$\mathrm{Nu}_x = \frac{x q_h}{k_f(T_w - T_\infty)},$$

$$\mathrm{Be} = \frac{\text{EG due to heat transfer}}{\text{Total EG}},$$

$$\tau_{wx} = \mu_{\mathrm{hnf}}\left(\frac{\partial u}{\partial z}\right)_{z=0},$$

$$\tau_{wy} = \mu_{\mathrm{hnf}}\left(\frac{\partial v}{\partial z}\right)_{z=0},$$

$$q_h = -k_{\mathrm{hnf}}\left(\frac{\partial T}{\partial z}\right)_{z=0}. \tag{35}$$

The aforementioned quantities in equations (33) and (34) utilizing Reynold's numbers $\mathrm{Re}_x = x u_w/\vartheta_f$ and $\mathrm{Re}_y = y v_w/\vartheta_f$ are expressed as

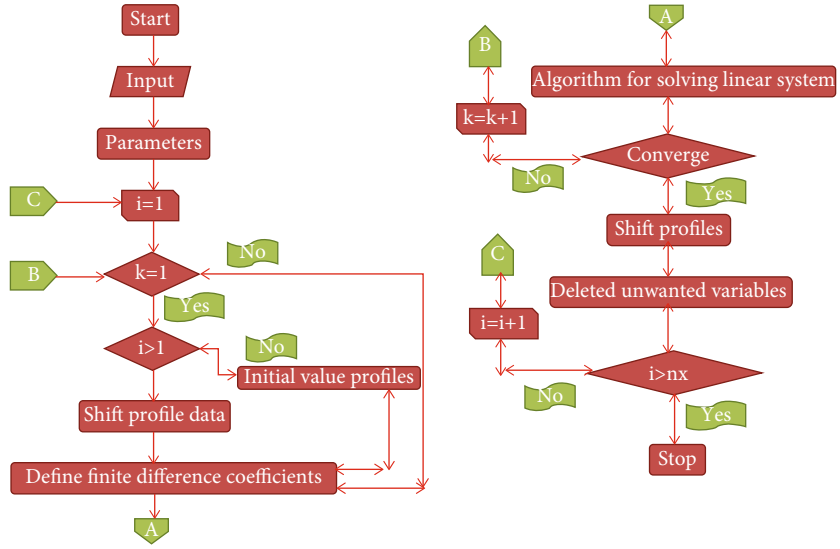

Figure 2: Flow chart for the Keller-Box simulation.

$$\begin{aligned}
\mathrm{Re}_x^{1/2} C_{fx} &= \varepsilon_5 f''(0), \\
\mathrm{Re}_y^{1/2} C_{fy} &= \alpha^{-3/2} \varepsilon_5 g''(0), \\
\mathrm{Re}_x^{-1/2} \mathrm{Nu}_x &= \begin{cases} -\dfrac{k_{hnf}}{k_f}\theta'(0) & \text{(VST case)}, \\ \dfrac{k_{hnf}}{k_f}\left(\dfrac{1}{\phi(0)}\right) & \text{(VHF case)}, \end{cases} \\
\mathrm{Be}_1|_{\mathrm{VST\ case}} &= \frac{\mathrm{Re}_x\theta'^2 + r^2\theta^2 + s^2\theta^2}{\mathrm{Re}_x\theta'^2 + r^2\theta^2 + s^2\theta^2 + (\mathrm{Re}_x B_r/\alpha_1)\left[M\varepsilon_4 f'^2 + \varepsilon_5 f''^2\right] + (\mathrm{Re}_y B_r/\alpha_1)\left[M\varepsilon_4 g'^2 + \varepsilon_5 g''^2\right]}, \\
\mathrm{Be}_2|_{\mathrm{VHF\ case}} &= \frac{\mathrm{Re}_x\phi'^2 + r^2\phi^2 + s^2\phi^2}{\mathrm{Re}_x\phi'^2 + r^2\phi^2 + s^2\phi^2 + (\mathrm{Re}_x B_r/\alpha_1)\left[M\varepsilon_4 f'^2 + \varepsilon_5 f''^2\right] + (\mathrm{Re}_y B_r/\alpha_1)\left[M\varepsilon_4 g'^2 + \varepsilon_5 g''^2\right]}.
\end{aligned} \tag{36}$$

3. Keller-Box Simulation

The next task after the mathematical modeling of the physical model is to construct the solution of the modeled equations. Here, we preferred the implicit finite difference technique, namely, the Keller-Box method, for the numerical solution of the modeled equations because it has second-degree accuracy with the flexibility of step size adoption. This method is most suitable for the solution of boundary layer flow problems because of its faster convergence rate as compared to ordinary numerical approaches (i.e., shooting method, BVP4c, and RK method). By using this method, the higher-order differential equations are converted to first-order differential equations, and then the first-order differential equations are transformed into difference equations by using central difference formulae. The difference equations are converted into linearized forms by means of Newton's linearization approach, and then these equations are arranged into the matrix-vector form. The solution of the matrix-vector form of linearized equations is obtained by using the LU decomposition method. In the whole process of the numerical solution, the physical domain $[0\infty)$ is shortened to the finite domain $[\eta_0\, \eta_\infty]$ by adjusting $\eta_0 = 0$, $\eta_\infty = 20$, $n_p = 500$, and $h = (\eta_\infty - \eta_0)/n_p$ to obtain the first approximation of the numerical solution, and then the numbers of grid points n_p are increased by reducing the step size h to achieve the desired accuracy, i.e., $\varepsilon = 10^{-6}$. The complete description of the Keller-Box simulation/numerical code is presented via a flow chart (Figure 2).

Table 2: Keller-Box solution of the present mathematical model using the grid-independent approach when $\alpha = S = M = 0.5$, $r = s = 1.0$, and $\psi_1 = \psi_2 = 0.02$.

Grid points: n_p	$-f''(0)$	$-g''(0)$	$-\theta'(0)$	$\phi(0)$
500	1.423414	0.639961	3.502719	0.285493
1000	1.423413	0.639953	3.502253	0.28553
1500	1.423413	0.639952	3.502167	0.285538
2000	1.423413	0.639951	3.502137	0.28554
2500	1.423413	0.639951	3.502123	0.285541
3000	1.423413	0.639951	3.502115	0.285542
3500	1.423413	0.639951	3.50211	0.285542
4000	1.423413	0.639951	3.502107	0.285542
4500	1.423413	0.639951	3.502105	0.285542
5000	1.423413	0.639951	3.502105	0.285542
10,000	1.423413	0.639951	3.502105	0.285542

The grid-independent solution of the modeled problem via the Keller-Box method is presented in Table 2 for suitable choices of involved physical parameters with the help of thermophysical features of water, magnetite, and silver. Table 2 discloses that with the upgradation of grid points, the solution approaches its convergence criterion. 1000 grid points are enough for the convergence of $f''(0)$, 2000 grid points are enough for the convergence of $g''(0)$, 5000 grid points are sufficient for the convergence of $\theta'(0)$, and 3000 grid points are necessary for the convergence of $\phi(0)$. However, the Keller-Box solution of the mathematical model is presented with up to 10,000 grid points for the declaration of its stability. This grid-independent

Table 3: Robust validation of the present outcomes with previous investigations when $S = M = \psi_1 = \psi_2 = 0.0$.

	$f(\infty)$	$g(\infty)$	$-f''(0)$	$-g''(0)$
$\alpha = 1.0$				
Current outcomes	0.751494	0.751494	1.173721	1.173721
Liu and Andersson [27]	0.751494	0.751494	1.173721	1.173721
Wang [53]	0.751527	0.751527	1.173720	1.173720
$\alpha = 0.5$				
Current outcomes	0.842360	0.451663	1.093096	0.465206
Liu and Andersson [27]	0.842360	0.451663	1.093096	0.465206
Wang [53]	0.842360	0.451671	1.093097	0.465205
$\alpha = 0.0$				
Current outcomes	1.0	0.0	-1.0	0.0
Liu and Andersson [27]	1.0	0.0	-1.0	0.0
Wang [53]	1.0	0.0	-1.0	0.0

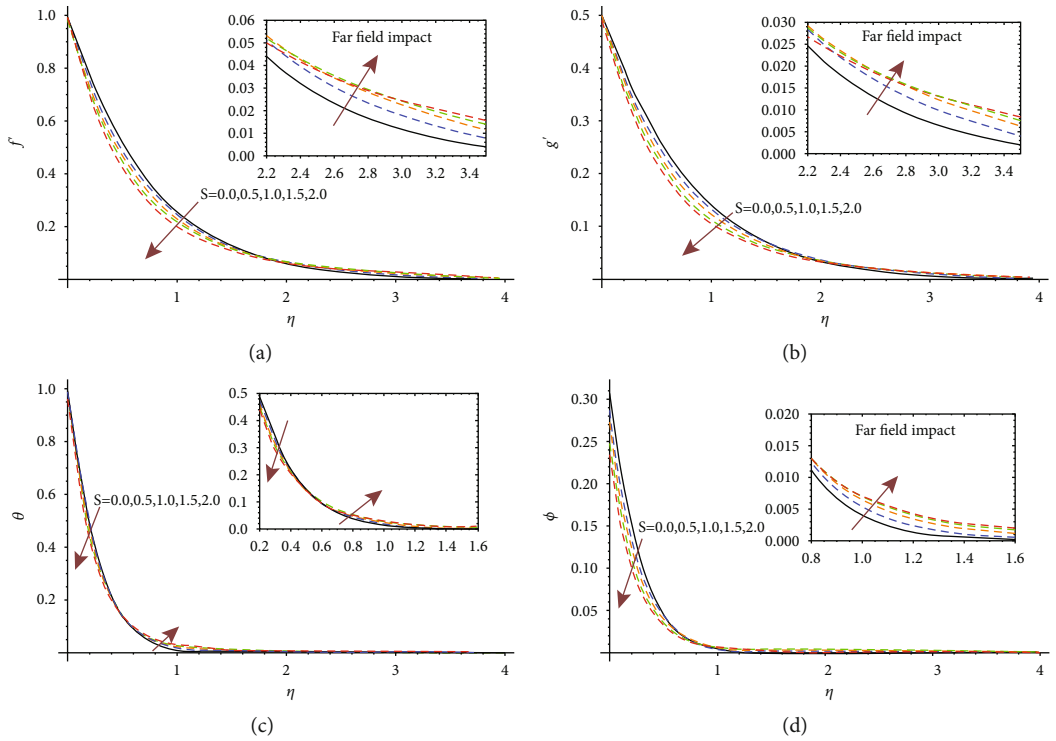

Figure 3: (a–d) The impact of the unsteady factor on $f'(\eta)$ via panel (a), on $g'(\eta)$ via panel (b), on $\theta(\eta)$ via panel (c), and on $\phi(\eta)$ via panel (d).

solution is further used to manipulate the outcomes for physical quantities of thermal importance and for graphical illustrations against various choices of pertinent involved entities.

3.1. Robust Validation. In order to the validation of the numerical technique using the grid-independent approach, a restricted comparison is incorporated with the existing literature by using 10,000 grid points in Table 3. A convincing pact is found among current scrutiny and previous investigations.

4. Results and Discussion

The major and foremost outcomes of the present investigation are discussed in this section of the report in the form of tables and various graphical representations. The impact of unsteady factor S on hybrid nanofluid velocity component $f'(\eta)$, velocity component $g'(\eta)$, thermal setup $\theta(\eta)$ for the VST environment, and thermal setup $\phi(\eta)$ for the VHF environment is discussed through Figures 3(a)–3(d), respectively. It is observed through Figures 3(a)–3(d) that the progression in the choice of

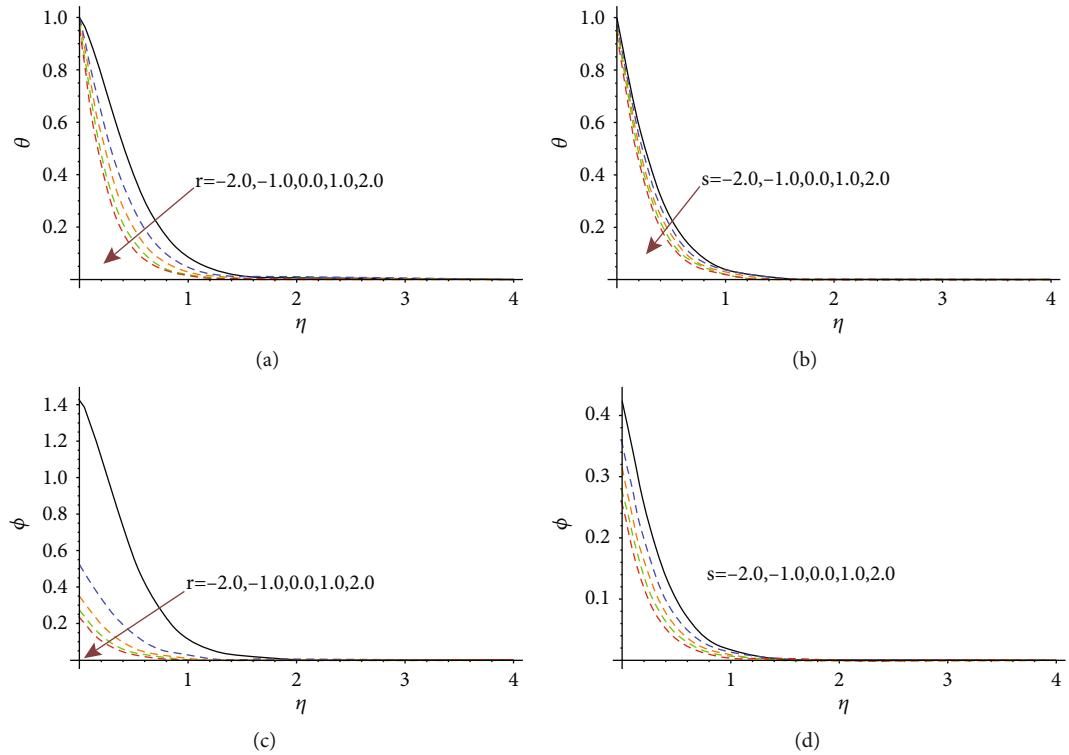

FIGURE 4: (a–d) Impacts of indices r on $\theta(\eta)$ via panel (a), s on $\theta(\eta)$ via panel (b), r on $\phi(\eta)$ via panel (c), and s on $\phi(\eta)$ via panel (d).

the unsteady factor from $S = 0.0 - 2.0$ reduces the impact of velocities f' and g', impact of thermal setup $\theta(\eta)$ for the VST approach, and impact of thermal setup $\phi(\eta)$ for the VHF approach nearer to the stretching device. Opposite trends are noticed in the far-field environment. Physically, the unsteady factor is the ratio of the dimensional constant c to the expansion rate a, and thus, the escalation in the choice of S produces a lower expansion rate and enhances the impact of c (i.e., positive expansion). Mathematically, the unsteady factor is also involved in the modeled equations in the product form with the quantities $f'(\eta)$, $g'(\eta)$, $\theta(\eta)$, and $\phi(\eta)$, respectively. As a result, these quantities are reduced with the escalation in the choice of the unsteady factor nearer to the stretching device. Moreover, the thickness of the boundary stream is also reduced with the improvement in the choice of the unsteady factor.

The significance of temperature-controlling indices r and s on the thermal setup is discussed in Figures 4(a) and 4(b) for the VST environment and Figures 4(c) and 4(d) for the VHF environment. It is noticed through these figures that intensifying choices of r and s diminish the thermal setup for both the prescribed heating mechanisms. Physically, r and s are involved in the energy equation as the product of $\theta(\eta)$ and $\phi(\eta)$, that is, the main cause of temperature reduction. Moreover, negative choices of r and s produce more temperature distribution than positive choices of r and s. Furthermore, the temperature distribution is activated higher for the VHF environment than the VST environment for $r = -2$, whereas it is triggered higher for VST aspects than VHF aspects for all the adopted choices of the index s. The augmentation in the choice of r reduces the thickness of the thermal layer, and the thickness of the thermal layer dominates for the diverse considerations of r than the considerations of s (i.e., thermal index along the y-direction). Figure 5(a) accompanies the significance of M and implication of α on $f'(\eta)$. The first velocity component $f'(\eta)$ is abbreviated with the enlargement of M from $M = 0.0 - 1.6$ and amplification of α for $\alpha = 0.4$ and $\alpha = 0.7$ (i.e., dashed lines). Physically, the stretching rate a lies in the denominator of both factors M and α, and therefore, the reduction to $f'(\eta)$ can be observed.

Figure 5(b) conveys the importance of M and inference of α on $g'(\eta)$. The second velocity component $g'(\eta)$ is abridged with the development of M from $M = 0.0 - 1.6$, and it is enhanced with the magnification of α for $\alpha = 0.4$ and $\alpha = 0.7$ (i.e., dashed lines). Physically, the stretching rate b lies in the numerator of α, whereas the stretching rate a deceits in the denominator of M (i.e., magnetic parameter). Therefore, the proliferation in $g'(\eta)$ is noticed for α and reduction in $g'(\eta)$ is observed for the magnetic factor. The thickness of the momentum layer is also improved due to the resistivity impact of the Lorentz force. Figure 5(c) illustrates the consequence of M and significance of α on $\theta(\eta)$. Temperature $\theta(\eta)$ is condensed with the progression of α, whereas it is intensified with the evolution of the magnetic factor. Physically, the Lorentz force slows down the velocity of the hybrid nanofluid and gave the domination chance to $\theta(\eta)$ (i.e., temperature for the VST process). Figure 5(d) elucidates the importance of M and worth of α on $\phi(\eta)$. Temperature $\phi(\eta)$ is shortened with the evolution of α, whereas it is deepened with the advancement of the magnetic feature. Actually, the Lorentz force acts as a resistive agent for

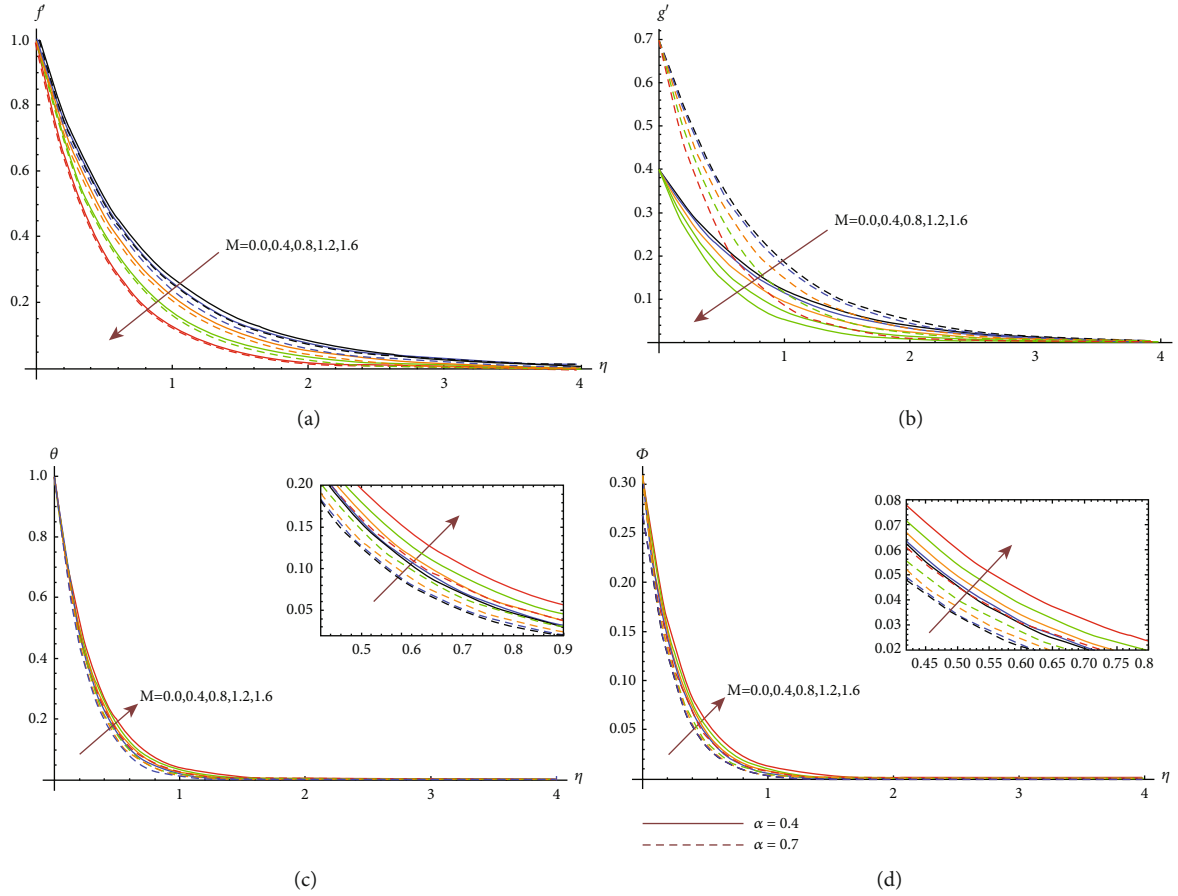

Figure 5: (a–d) Impacts of M and α on $f'(\eta)$ via panel (a), on $g'(\eta)$ via panel (b), on $\theta(\eta)$ via panel (c), and on $\phi(\eta)$ via panel (d).

Table 4: Significance of nanoparticle volume fractions ψ_1 and ψ_2 on the physical quantities having thermal engineering interests when $\alpha = S = M = 0.5$ and $r = s = 1.0$.

Nanoparticle volume fractions		$-\mathrm{Re}_y^{1/2} C_{fx}$	$-\mathrm{Re}_y^{1/2} C_{fy}$	$\mathrm{Re}_x^{-1/2} \mathrm{Nu}_x$
ψ_1	ψ_2			
0.01	0.01	1.456536	1.853745	3.855186
0.03	0.01	1.54797	1.969733	3.903703
0.05	0.01	1.643119	2.090527	3.951304
0.07	0.01	1.742064	2.216231	3.997992
0.07	0.03	1.898586	2.412816	4.046919
0.07	0.05	2.058013	2.613309	4.094455
0.07	0.07	2.221041	2.818552	4.140588

the velocity of the hybrid mixture, and hence, $\phi(\eta)$ is increased with its positive approach.

Table 4 provides the significance of magnetite tiny particle volume fraction ψ_1 and silver tiny particle volume fraction ψ_2 on the skin friction coefficients and local Nusslet number for fixed choices of other involved entities. It is elaborated in Table 4 that higher choices of ψ_1 and ψ_2

Table 5: Variation in the thermophysical features for the present mixture of substances with $\psi_1 = 0.01$.

ψ_2	ρ_{hnf}	$(\rho C_p)_{\mathrm{hnf}} \times 10^3$	$k_{\mathrm{hnf}} \times 10^{-1}$	$\sigma_{\mathrm{hnf}} \times 10^{-2}$
0.00	1038.929	4.14391	6.284229742	5.151514233
0.01	1133.958	4.10447	6.473818137	5.307620725
0.03	1324.016	4.02559	6.864669077	5.629489779
0.05	1514.074	3.94671	7.271901012	5.964911215
0.07	1704.132	3.86783	7.696565802	6.31475938
0.09	1894.19	3.78895	8.139807334	6.679985485

Table 6: Variation in the thermophysical features for the present mixture of substances with $\psi_2 = 0.01$.

ψ_1	ρ_{hnf}	$(\rho C_p)_{\mathrm{hnf}} \times 10^3$	$k_{\mathrm{hnf}} \times 10^{-1}$	$\sigma_{\mathrm{hnf}} \times 10^{-2}$
0.00	1092.129	4.13956	6.31495557	5.151515151
0.01	1133.958	4.10447	6.473818137	5.307620725
0.03	1217.616	4.03429	6.799670393	5.629487827
0.05	1301.274	3.96411	7.136828795	5.964907143
0.07	1384.932	3.89393	7.485892168	6.134753003
0.09	1468.59	3.82375	7.487502391	6.679976602

Table 7: Percent-wise heat transport calculation for the various possessions of nanoparticles, $\alpha = S = M = 0.5$ and $r = s = 1.0$, by using the following formulae, i.e., %Increase = ((With nanoparticles − Without nanoparticles)/Without nanoparticles) × 100 = Result and % Enhancement = Result − 100%.

ψ_1, ψ_2	$\mathrm{Re}_x^{-1/2}\mathrm{Nu}_x$	
	$\mathrm{Fe_3O_4}(\psi_2 = 0.0)$	$\mathrm{Ag}(\psi_1 = 0.0)$
0.00	3.789531	3.789531
0.01	3.813768 (0.6395778% increase)	3.814161 (0.6499485% increase)
0.02	3.837764 (1.272796% increase)	3.838539 (1.2932471% increase)
0.04	3.885047 (2.520523% increase)	3.886515 (2.5592613% increase)
0.06	3.931391 (3.7434712% increase)	3.933425 (3.7971453% increase)
0.08	3.976797 (4.9416669% increase)	3.979245 (5.0062659% increase)

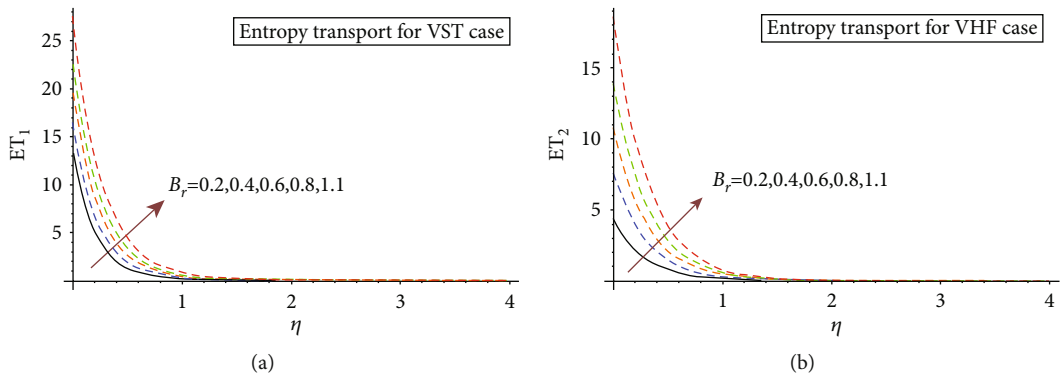

Figure 6: (a, b) Entropy transport for the variation of the Brinkman number.

enhance the worth of skin friction coefficients. Mathematically, the skin friction coefficients consist of the factor of tiny particle volume fractions, and therefore, strictly increasing behavior in the amount of skin friction is achieved with the development of volume fractions of tiny particles. Moreover, the skin friction coefficient is detected higher for the y-direction as compared to the x-direction as its mathematical expression involves the term of expansion ratio α with negative fraction power. The rate of heat transference is increased for both $0.01 \leq \psi_1 \leq 0.07$ and $0.01 \leq \psi_2 \leq 0.07$. Physically, the rate of heat transference depends on the value of thermal conductivity for magnetite and silver nanoparticles. As the thermal conductivity is higher for silver, silver is higher than magnetite, and therefore, silver nanoparticles have produced a faster rate of heat transference as compared to magnetite nanoparticles. Table 5 provides the impact of volume fraction ψ_2 on the thermophysical features of hybrid nanofluid with the present mixture of the substances, whereas Table 6 discloses the effect of volume fraction ψ_1 on the thermophysical features of hybrid nanofluid with the mixture of water, magnetite, and silver. It is noticed through these tables that higher choices of ψ_1 and ψ_2 reduce the effective heat capacity of hybrid nanofluid, whereas the escalating amounts of these substances (magnetite and silver) boost the worth of thermal conductivity, density, and electrical conductivity of the hybrid nanofluid. These outcomes are favorable for a lot of industrial and engineering applications. Table 7 is included to discuss the percentage increase in the rate of heat transport for the suspensions of magnetite and silver in the host liquid, i.e., water. According to the calculated results, silver is more reliable and efficient in order to enhance the rate of heat transport than magnetite. Physically, the thermal conductivity of silver is much higher than that of magnetite, and so the percent-wise enhancement in the rate of heat transport is observed to be higher for silver nanoparticles.

Figure 6(a) is included to discuss the control of Brinkman number B_r on entropy transport for the VST case, whereas Figure 6(b) illustrates its impact on entropy transport for the VHF case. Entropy is augmented with the upgradation of B_r from $B_r = 0.2 - 1.1$, and the worth of this augmentation is almost doubled for the VST case as compared to the VHF case. Physically, the velocity of the fluid enhances with the progression of B_r and declines with the augmentation of the temperature difference between the wall and the far-field. So, these spectacular trends are achieved with the variation of the Brinkman number. Figure 7(a) is incorporated to confer the influence of temperature difference parameter α_1 on the Bejan number for the VST case, whereas Figure 7(b) elucidates its impression on the Bejan number for the VHF case. The Bejan number is amplified with the evolution of α_1 from $\alpha_1 = 0.1 - 0.9$, and the net impact of this intensification is almost doubled for the VST case as compared to the VHF case. Physically, the far-field temperature contracts with the advancement of α_1 and amplifies with the growth of the temperature difference between the wall and the far-field. So, these enormous tendencies are attained with the variant of the temperature difference parameter.

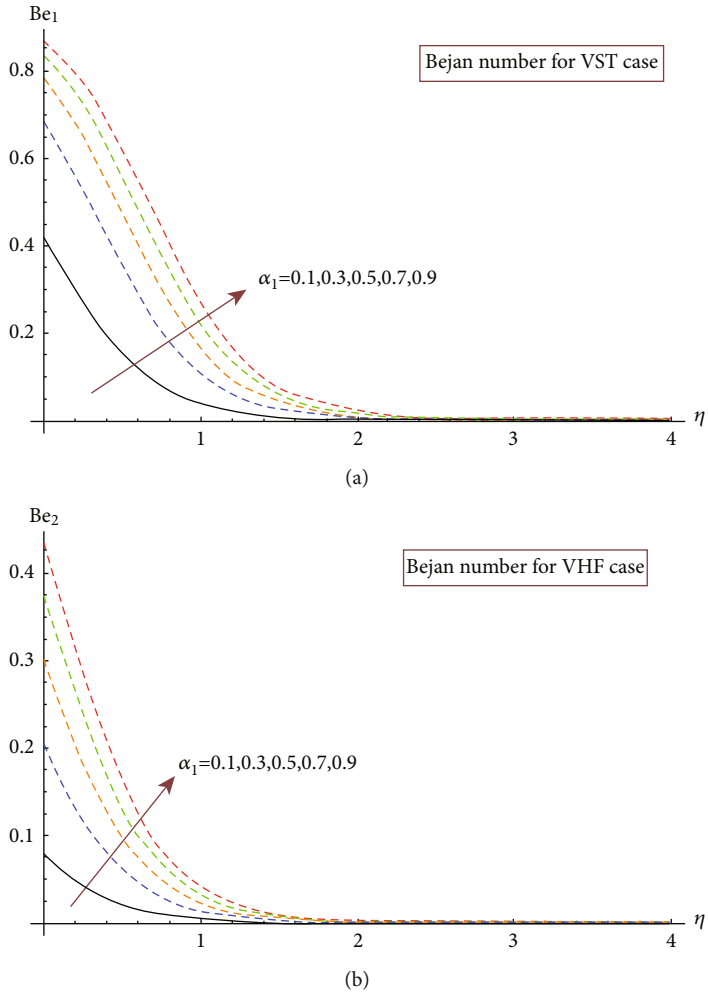

Figure 7: (a, b) Bejan number for the variation of the temperature difference parameter.

5. Conclusions

Heat transport and entropy transport in bidirectional hybrid nanofluid containing nanospheres (magnetite and silver) with VST (variable surface temperature) and VHF (variable surface heat flux) mechanisms are scrutinized. The Hamilton-Crosser nanofluid model is used to inspect the impact of nanospheres. Water is considered the base fluid with the amalgamations of nanospheres. The Keller-Box method has been used to solve the modeled problem, and outcomes have been discussed graphically as well as in tabular arrangements. The pertinent observations are as follows:

(i) The velocity setup for the present mixture of nanospheres into the host liquid remains on the inferior side

(ii) The reduction in the thermal setup has been chronicled for the amplification in the choices of heat distribution indices

(iii) The Nusselt number for the present combination of nanospheres shows its proficiency for escalating nanosphere volume fractions

(iv) The nanospheres play a vital role in the improvement of the thermal conductivity of hybrid nanofluid

(v) Percentage enhancement in the rate of heat transport is observed to be higher for silver nanospheres as compared to magnetite nanospheres

(vi) Entropy is amplified with the positive estimation of the Brinkman number, and the Bejan number is also amplified with the positive tendency of the temperature difference parameter

The outcomes of the present investigation are helpful in the development of heat exchangers, coating a sheet with nanoparticles, the purification process of water, steel manufacturing, drug delivery, etc.

Nomenclature

(x, y, z): Cartesian configuration
(u, v, w): Velocity field components
t: Time
T: Temperature

η: Similarity variable
(f, g, θ): Similarity functions
(r, s): Indices
Pr: Prandtl number
ET: Entropy transport
E_c: Characteristic entropy
VST: Variable surface temperature
ET_1: Entropy for the VST case
VHF: Variable surface heat flux
ET_2: Entropy for the VHF case
(a, b): Stretching rates
c: Positive constant
B_0: Magnetic field strength
(u_w, v_w): Stretching velocities
H_2O: Water
Fe_3O_4: Magnetite
Ag: Silver
ρ: Density
k: Thermal conductivity
C_p: Specific heat
σ: Electrical conductivity
μ: Dynamic viscosity
bf: Base fluid
hnf: Hybrid nanofluid
ψ_1: Concentration of magnetite nanospheres
ψ_2: Concentration of silver nanospheres
ϑ_f: Kinematic viscosity of fluid
S: Unsteady parameter
M: Magnetic parameter
α: Bidirectional stretching parameter
$\varepsilon_i, i = 1 - 5$: Hybrid nanofluid coefficients
q_w: Heat flux
(T_0, T_1): Dimensional constants
T_w: Surface temperature
(Re_x, Re_y): Reynold's numbers
T_∞: Ambient temperature
B_r: Brinkman number
α_1: Temperature difference parameter
(C_{fx}, C_{fy}): Skin friction coefficients
Nu_x: Nusselt number
(Be_1, Be_2): Bejan numbers
h: Step size
ε: Convergence criterion.

Data Availability

The raw data supporting the conclusion of this report will be made available by the corresponding author without undue reservation.

Conflicts of Interest

The authors declare that there is no conflict of interest.

Authors' Contributions

All authors contributed equally to this work. And all the authors have read and approved the final version manuscript.

References

[1] S. U. S. Choi, Z. G. Zhang, W. Yu, F. E. Lockwood, and E. A. Grulke, "Anomalous thermal conductivity enhancement in nanotube suspensions," *Applied Physics Letters*, vol. 79, no. 14, pp. 2252–2254, 2001.

[2] J. C. Maxwell, *A Treatise on Electricity and Magnetism (Vol. 1)*, Clarendon Press, Oxford, 1873.

[3] V. D. Bruggeman, "Berechnung verschiedener physikalischer Konstanten von heterogenen Substanzen. I. Dielektrizitätskonstanten und Leitfähigkeiten der Mischkörper aus isotropen Substanzen," *Annalen der Physik*, vol. 416, no. 7, pp. 636–664, 1935.

[4] R. L. Hamilton and O. K. Crosser, "Thermal conductivity of heterogeneous two-component systems," *Industrial & Engineering Chemistry Fundamentals*, vol. 1, no. 3, pp. 187–191, 1962.

[5] N. Masoumi, N. Sohrabi, and A. Behzadmehr, "A new model for calculating the effective viscosity of nanofluids," *Journal of Physics D: Applied Physics*, vol. 42, no. 5, article 055501, 2009.

[6] M. Mooney, "The viscosity of a concentrated suspension of spherical particles," *Journal of Colloid Science*, vol. 6, no. 2, pp. 162–170, 1951.

[7] H. Ohshima, "Effective viscosity of a concentrated suspension of uncharged spherical soft particles," *Langmuir*, vol. 26, no. 9, pp. 6287–6294, 2010.

[8] X. Zhang, H. Gu, and M. Fujii, "Effective thermal conductivity and thermal diffusivity of nanofluids containing spherical and cylindrical nanoparticles," *Journal of Applied Physics*, vol. 100, no. 4, article 044325, 2006.

[9] S. Saleem, I. L. Animasaun, S. J. Yook, Q. M. Al-Mdallal, N. A. Shah, and M. Faisal, "Insight into the motion of water conveying three kinds of nanoparticles shapes on a horizontal surface: significance of thermo-migration and Brownian motion," *Surfaces and Interfaces*, vol. 30, article 101854, 2022.

[10] E. V. Timofeeva, J. L. Routbort, and D. Singh, "Particle shape effects on thermophysical properties of alumina nanofluids," *Journal of Applied Physics*, vol. 106, no. 1, article 014304, 2009.

[11] K. Yang and Y. Q. Ma, "Computer simulation of the translocation of nanoparticles with different shapes across a lipid bilayer," *Nature Nanotechnology*, vol. 5, no. 8, pp. 579–583, 2010.

[12] I. Ahmad, M. Faisal, Q. Zan-Ul-Abadin, T. Javed, and K. Loganathan, "Unsteady 3D heat transport in hybrid nanofluid containing brick shaped ceria and zinc-oxide nanocomposites with heat source/sink," *Nano*, vol. 8, no. 1, pp. 1–12, 2022.

[13] S. S. U. Devi and S. A. Devi, "Numerical investigation of three-dimensional hybrid $Cu–Al_2O_3$/water nanofluid flow over a stretching sheet with effecting Lorentz force subject to Newtonian heating," *Canadian Journal of Physics*, vol. 94, no. 5, pp. 490–496, 2016.

[14] T. Hayat, S. Nadeem, and A. U. Khan, "Rotating flow of Ag-CuO/H_2O hybrid nanofluid with radiation and partial slip boundary effects," *The European Physical Journal E*, vol. 41, no. 6, pp. 1–9, 2018.

[15] V. Kumar and R. R. Sahoo, "Viscosity and thermal conductivity comparative study for hybrid nanofluid in binary base fluids," *Research*, vol. 48, no. 7, pp. 3144–3161, 2019.

[16] M. F. Nabil, W. H. Azmi, K. A. Hamid, N. N. M. Zawawi, G. Priyandoko, and R. Mamat, "Thermo-physical properties of hybrid nanofluids and hybrid nanolubricants: a comprehensive review on performance," *International Communications in Heat and Mass Transfer*, vol. 83, pp. 30–39, 2017.

[17] U. Rashid and H. Liang, "Investigation of nanoparticles shape effects on MHD nanofluid flow and heat transfer over a rotating stretching disk through porous medium," *International Journal of Numerical Methods for Heat & Fluid Flow*, vol. 30, no. 12, pp. 5169–5189, 2020.

[18] H. A. Nabwey and A. Mahdy, "Transient flow of micropolar dusty hybrid nanofluid loaded with Fe_3O_4-Ag nanoparticles through a porous stretching sheet," *Results in Physics*, vol. 21, article 103777, 2021.

[19] N. A. Zainal, R. Nazar, K. Naganthran, and I. Pop, "Heat generation/absorption effect on MHD flow of hybrid nanofluid over bidirectional exponential stretching/shrinking sheet," *Chinese Journal of Physics*, vol. 69, pp. 118–133, 2021.

[20] N. Ahmed, F. Saba, U. Khan et al., "Spherical shaped (Ag $-Fe_3O_4/H_2O$) hybrid nanofluid flow squeezed between two Riga plates with nonlinear thermal radiation and chemical reaction effects," *Energies*, vol. 12, no. 1, pp. 1–23, 2019.

[21] G. Sowmya, B. J. Gireesha, I. L. Animasaun, and N. A. Shah, "Significance of buoyancy and Lorentz forces on water-conveying iron(III) oxide and silver nanoparticles in a rectangular cavity mounted with two heated fins: heat transfer analysis," *Journal of Thermal Analysis and Calorimetry*, vol. 144, no. 6, pp. 2369–2384, 2021.

[22] N. Acharya, F. Mabood, and I. A. Badruddin, "Thermal performance of unsteady mixed convective Ag/MgO nanohybrid flow near the stagnation point domain of a spinning sphere," *International Communications in Heat and Mass Transfer*, vol. 134, article 106019, 2022.

[23] F. Ali, K. Loganathan, S. Eswaramoorthi, K. Prabu, A. Zaib, and D. K. Chaudhary, "Heat transfer analysis on carboxymethyl cellulose water-based cross hybrid nanofluid flow with entropy generation," *Journal of Nanomaterials*, vol. 2022, Article ID 5252918, 11 pages, 2022.

[24] K. Thriveni and B. Mahanthesh, "Sensitivity computation of nonlinear convective heat transfer in hybrid nanomaterial between two concentric cylinders with irregular heat sources," *International Communications in Heat and Mass Transfer*, vol. 129, article 105677, 2021.

[25] J. Mackolil and B. Mahanthesh, "Optimization of heat transfer in the thermal Marangoni convective flow of a hybrid nanomaterial with sensitivity analysis," *Applied Mathematics and Mechanics*, vol. 42, no. 11, pp. 1663–1674, 2021.

[26] J. L. G. Oliveira, C. Tecchio, K. V. Paiva, M. B. H. Mantelli, R. Gandolfi, and L. G. S. Ribeiro, "Passive aircraft cooling systems for variable thermal conditions," *Applied Thermal Engineering*, vol. 79, pp. 88–97, 2015.

[27] I. C. Liu and H. I. Andersson, "Heat transfer over a bidirectional stretching sheet with variable thermal conditions," *International Journal of Heat and Mass Transfer*, vol. 51, no. 15-16, pp. 4018–4024, 2008.

[28] I. Ahmad, M. Faisal, and T. Javed, "Dynamics of copper–water nanofluid with the significance of prescribed thermal conditions," *Heat Transfer*, vol. 50, no. 5, pp. 4248–4263, 2021.

[29] I. Ahmad, M. Faisal, and T. Javed, "Unsteady rotating flow of nanofluid with prescribed thermal aspects," *International Journal of Modern Physics C*, vol. 32, no. 7, article 2150093, 2021.

[30] I. Waini, A. Ishak, and I. Pop, "Hybrid nanofluid flow on a shrinking cylinder with prescribed surface heat flux," *International Journal of Numerical Methods for Heat & Fluid Flow*, vol. 31, no. 6, pp. 1987–2004, 2021.

[31] I. Waini, A. Ishak, and I. Pop, "Hybrid nanofluid flow and heat transfer past a vertical thin needle with prescribed surface heat flux," *International Journal of Numerical Methods for Heat & Fluid Flow*, vol. 29, no. 12, pp. 4875–4894, 2019.

[32] N. S. Khashi'ie, I. Waini, N. A. Zainal, K. Hamzah, and A. R. Mohd Kasim, "Hybrid nanofluid flow past a shrinking cylinder with prescribed surface heat flux," *Symmetry*, vol. 12, no. 9, p. 1493, 2020.

[33] B. J. Gireesha, B. Mahanthesh, and R. S. R. Gorla, "Suspended particle effect on nanofluid boundary layer flow past a stretching surface," *Journal of Nanofluids*, vol. 3, no. 3, pp. 267–277, 2014.

[34] I. Ahmad, M. Faisal, and T. Javed, "Bi-directional stretched nanofluid flow with Cattaneo-Christov double diffusion," *Results in Physics*, vol. 15, article 102581, 2019.

[35] T. Javed, M. Faisal, and I. Ahmad, "Dynamisms of solar radiation and prescribed heat sources on bidirectional flow of magnetized Eyring-Powell nanofluid," *Case Studies in Thermal Engineering*, vol. 21, article 100689, 2020.

[36] M. Turkyilmazoglu and I. Pop, "Heat and mass transfer of unsteady natural convection flow of some nanofluids past a vertical infinite flat plate with radiation effect," *International Journal of Heat and Mass Transfer*, vol. 59, pp. 167–171, 2013.

[37] T. Javed, M. Faisal, and I. Ahmad, "Dynamisms of activation energy and convective Nield's conditions on bidirectional flow of radiative Eyring–Powell nanofluid," *International Journal of Modern Physics C (IJMPC)*, vol. 31, no. 11, article 2050156, 2020.

[38] G. Huminic and A. Huminic, "Entropy generation of nanofluid and hybrid nanofluid flow in thermal systems: a review," *Journal of Molecular Liquids*, vol. 302, article 112533, 2020.

[39] M. I. Khan, M. U. Hafeez, T. Hayat, M. I. Khan, and A. Alsaedi, "Magneto rotating flow of hybrid nanofluid with entropy generation," *Computer Methods and Programs in Biomedicine*, vol. 183, article 105093, 2020.

[40] G. Huminic and A. Huminic, "The heat transfer performances and entropy generation analysis of hybrid nanofluids in a flattened tube," *International Journal of Heat and Mass Transfer*, vol. 119, pp. 813–827, 2018.

[41] S. Ahmad, S. Nadeem, and N. Ullah, "Entropy generation and temperature-dependent viscosity in the study of SWCNT–MWCNT hybrid nanofluid," *Applied Nanoscience*, vol. 10, no. 12, pp. 5107–5119, 2020.

[42] U. M. Zahid, Y. Akbar, and F. M. Abbasi, "Entropy generation analysis for peristaltically driven flow of hybrid nanofluid," *Chinese Journal of Physics*, vol. 67, pp. 330–348, 2020.

[43] A. A. Hussien, M. Z. Abdullah, N. M. Yusop, W. Al-Kouz, E. Mahmoudi, and M. Mehrali, "Heat transfer and entropy generation abilities of MWCNTs/GNPs hybrid nanofluids in microtubes," *Entropy*, vol. 21, no. 5, p. 480, 2019.

[44] M. Sheikholeslami, Z. Shah, A. Shafee, P. Kumam, and H. Babazadeh, "Lorentz force impact on hybrid nanofluid within a porous tank including entropy generation," *International Communications in Heat and Mass Transfer*, vol. 116, article 104635, 2020.

[45] H. Upreti, A. K. Pandey, and M. Kumar, "Assessment of entropy generation and heat transfer in three-dimensional

hybrid nanofluids flow due to convective surface and base fluids," *Journal of Porous Media*, vol. 24, no. 3, pp. 35–50, 2021.

[46] B. Saleh and L. S. Sundar, "Entropy generation and exergy efficiency analysis of ethylene glycol-water based nanodiamond + Fe_3O_4 hybrid nanofluids in a circular tube," *Powder Technology*, vol. 380, pp. 430–442, 2021.

[47] S. Eswaramoorthi, S. Divya, M. Faisal, and N. Namgyel, "Entropy and heat transfer analysis for MHD flow of-water-based nanofluid on a heated 3D plate with nonlinear radiation," *Mathematical Problems in Engineering*, vol. 2022, Article ID 7319988, 14 pages, 2022.

[48] M. Faisal, I. Ahmad, and T. Javed, "Keller-Box simulation for nonzero and zero mass fluxes of nanofluid flow impinging over a bi-directional stretching sheet: an unsteady mathematical model," *International Journal of Modern Physics C*, vol. 32, no. 4, article 2150052, 2021.

[49] I. Ahmad, M. Faisal, and T. Javed, "Magneto-nanofluid flow due to bidirectional stretching surface in a porous medium," *Special Topics & Reviews in Porous Media: An International Journal*, vol. 10, no. 5, pp. 457–473, 2019.

[50] M. Faisal, I. Ahmad, and T. Javed, "Radiative nanofluid flow due to unsteady bi-directional stretching surface with convective and zero mass flux boundary conditions: using Keller Box scheme," *Computational Thermal Sciences: An International Journal*, vol. 12, no. 4, pp. 361–385, 2020.

[51] T. Javed, M. Faisal, and I. Ahmad, "Actions of viscous dissipation and ohmic heating on bidirectional flow of a magneto-Prandtl nanofluid with prescribed heat and mass fluxes," *Heat Transfer*, vol. 49, no. 8, pp. 4801–4819, 2020.

[52] M. Faisal, I. Ahmad, and T. Javed, "Numerical simulation of mixed convective 3D flow of a chemically reactive nanofluid subject to convective Nield's conditions with a nonuniform heat source/sink," *Heat Transfer*, vol. 50, no. 1, pp. 352–369, 2021.

[53] C. Y. Wang, "The three-dimensional flow due to a stretching flat surface," *The Physics of Fluids*, vol. 27, no. 8, pp. 1915–1917, 1984.